Article

Journal of Vibration and Control
2022, Vol. 0(0) 1–13

DOI: 10.1177/1077546322113561 7
journals.sagepub.com/home/jvc
SAGE

Study of chattering suppression for the sliding mode controller of an electromagnetic levitation system

Weiwei ZHANG[1,2], Han WU[1,3], Xiaohui ZENG[1,3], and Mengjuan LIU[1,3]

Abstract

Due to the inherent non-linearity and open-loop instability of maglev systems, their high-quality control performance is critical in the development stage. Sliding mode control has great potential in the field of maglev vehicle control because of its superior control performance, robustness and interference resistance. In practical applications of sliding mode control, however, the limitations of the hardware physical properties and time delay of the control units of maglev systems can cause chattering, thereby significantly reducing the stability of maglev vehicles. In order to suppress chattering, a modified sliding mode controller that combines the exponential reaching law and continuous control laws is proposed in this study. A single-point levitation experimental platform and corresponding co-simulation model were built, and a parameter influence analysis of the modified sliding mode controller was conducted. This paper presents an adaptive correction method for the sliding mode control parameters based on the aforementioned chattering study. The actual levitation experiments were used to validate the control performance of the proposed controllers. Overall, the conducted research revealed that the modified controllers could effectively suppress chattering and possess excellent robustness.

Keywords

maglev vehicle, sliding mode control, rapid control prototyping, hardware experiments, non-linear control law

1. Introduction

Electromagnetic suspension (EMS) maglev vehicles have the advantages of high speed, low noise and low maintenance because of their contactless property, which is in line with the development trend of green and intelligent transportation systems. The electromagnetic levitation of EMS maglev vehicles is open-loop unstable and inherently non-linear, where their levitation stability depends on the active control of the electromagnetic force. Therefore, control algorithms are essential for electromagnetic levitation systems.

Traditional control algorithms, which are mostly based on the linear theory (Su et al., 2005), have limitations for high control requirements. In practical engineering applications, the mechanical environment of maglev vehicles is still complex, as the associated aerodynamic effects grow rapidly and fluctuate non-linearly with the increase in speed. The aerodynamic effect around high-speed trains tends to be obvious with the increase in speed, resulting in changes in the dynamic characteristics of high-speed trains (Wu et al., 2020b; Zeng et al., 2021). Moreover, Wu et al. (2021); Wu et al. (2020a) found that the steady development of aerodynamic effects in the high-speed stage affects the stability of the time delay maglev systems with feedback control. Additionally, linear control may encounter difficulties with regard to track irregularity and vehicle-bridge coupling vibration (Li et al., 2020; Wang et al., 2020a). Maglev systems are altogether naturally non-linear. Furthermore, their complex mechanical

[1]Key Laboratory for Mechanics in Fluid Solid Coupling Systems, Institute of Mechanics, Chinese Academy of Sciences, Beijing, China
[2]School of Future Technology, University of Chinese Academy of Sciences, Beijing, China
[3]School of Engineering Science, University of Chinese Academy of Sciences, Beijing, China

Received: 5 June 2022; accepted: 3 October 2022

Corresponding author:
Han WU, Key Laboratory for Mechanics in Fluid Solid Coupling Systems, Institute of Mechanics, Chinese Academy of Sciences, China, No.15 Beisihuanxi Road, Beijing 100190, China.
Email: wuhan@imech.ac.cn

environment accentuates their non-linearity, making linear control difficult to stabilize the vehicles near nominal clearance. Thus, it is vital to develop a non-linear control algorithm with better robustness so as to avoid performance reduction.

Sliding mode control (SMC), as an intelligent control algorithm, is well suited for the robust control of the high-order non-linear systems under complex environments due to its excellent control performance and robustness. Nowadays, SMC is successfully applied in underwater vehicle (Roy and Ghoshal, 2021), electromagnetic bearing (Wang et al., 2020b) and maglev vehicle (De Boeij et al., 2006). The basic concept of SMC is that the ideal control law makes state trajectory converge asymptotically to the sliding mode surface in the state space. However, due to the practical time delay and the limitation of the electrical equipment, the unavoidable unmodeled dynamic characteristics, state trajectories cannot ideally switch at the sliding mode surface, resulting in undesirable high-frequency chattering. Not only does the problem degrade control quality severely and heat the electromagnet rapidly, but also it has the potential to excite unmodeled non-linear dynamics, resulting in further hazards. To suppress chattering, Slotine (1984) used the continuous control law to improve control performance. Bartolini et al. (1998); Ferrara et al. (2019) proposed a high-order SMC which requires more state information. For the complicated system with uncertainty in system characteristics and parameters, Eroglu and Ablay (2016) connected an integral SMC in series to compensate for errors. Xu et al. (2018) proposed a consistent flux observer to predict accurate models in real time for SMC. Sun et al. (2019a, 2019b, 2021) successfully applied radial basis function (RBF) neural network, neuro-fuzzy switching law and deep belief network (DBN) to adjust the SMC control parameters online.

The chattering issue is the greatest barrier impeding the widespread use of SMC. While scholars have previously applied sliding mode control to maglev control, they have not provided a viable solution to the chattering issue. In order to expand the use of the SMC approach in maglev control, it is important to develop an efficient way for suppressing chattering. To accomplish this, we analysed the parameter sensitivity of electromagnetic levitation system chattering for several sliding mode controllers. Following the results of the investigation, a simple and effective adaptive correction mechanism was proposed to further enhance the chattering suppression effect. Simulations and experiments on single-point levitation ultimately validated the chattering suppression capability of the modified sliding mode controller.

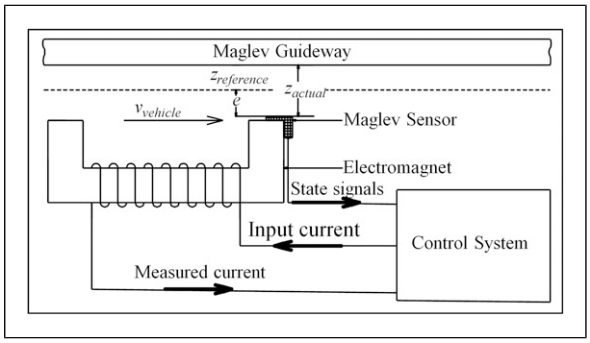

Figure 1. Schematic diagram of the single electromagnet levitation system.

2. Dynamic model of electromagnetic levitation

In the maglev vehicle system, each electromagnet is controlled by current from Figure 1. Experiments and theory have indicated that the whole maglev vehicle dynamic system can be decoupled into mutually independent single electromagnet levitation dynamic models (Xu et al., 2018). To facilitate the study of the non-linear characteristics of individual controlling units, the single electromagnet levitation dynamic model shown in Figure 1 was used. In addition, the guideway was assumed to be rigid.

The levitation controlling units change the electromagnetic force by adjusting the current of the electromagnets, the vertical electromagnet dynamic equation can be written as follows:

$$m\ddot{z}(t) = -F(i(t), z(t)) + mg + f_d \tag{1}$$

where f_d represents the external interference, m represents the electromagnet mass, i represents the actual current, z represents the actual air clearance and F represents the electromagnetic force.

The electromagnetic force can be expressed as follows:

$$F(i(t), z(t)) = \frac{\mu_0 N^2 A}{4}\left[\frac{i(t)}{z(t)}\right]^2 \tag{2}$$

In Equation (2), μ_0 is permeability in vacuum, A is the effective area of the electromagnet and N is the number of coils.

The relative order of the non-linear electromagnetic force and current is zero. After introducing the new variable u and substituting Equation (2) into Equation (1), the single electromagnet levitation dynamic model can be updated as follows:

$$\begin{cases} \dot{x}_1(t) = x_2(t) \\ \dot{x}_2(t) = -\dfrac{\mu_0 A N^2}{4m} u + g + \dfrac{f_d}{m} \end{cases} \tag{3}$$

$$x_1 = z(t), x_2 = \dot{z}(t), u(t) = \frac{i^2(t)}{x_1^2(t)}$$

3. Sliding mode controller design

3.1. Sliding mode controller using exponential reaching law

When controlling proceeds, the tracking error is defined as **E** for the description of the electromagnetic levitation performance. The control objective is to make the tracking error decay quickly and stably to 0 in a finite time.

$$\mathbf{E} = [\, e_1 \quad e_2 \,]^T = [\, x_1 - x_{d_1} \quad x_2 - x_{d_2} \,]^T \tag{4}$$

where e_1 represents the air clearance error, e_2 represents the velocity error, x_1 represents the actual air clearance, x_{d1} represents the nominal levitation clearance, x_2 represents the actual levitation velocity and x_{d2} represents the expected levitation velocity.

The governing equation of the single electromagnet levitation model is Equation (3), and the corresponding second-order sliding mode surface is defined as follows:

$$s(x_1, x_2, t) = \left(\frac{d}{dt} + c\right) e = ce + \dot{e}, c > 0 \tag{5}$$

According to the Routh–Hurwitz stability criterion, $c > 0$ should be satisfied to ensure asymptotic stability. Furthermore, an exponential reaching law is applied to improve the control algorithm chattering suppression ability:

$$\dot{s} = -\xi \mathrm{sgn}(s) - ks, \xi > 0, k > 0 \tag{6}$$

where ξ represents the switching control term coefficient, k represents the exponential reaching term coefficient and sgn(·) is the signum function. By combining Equation (3) and Equation (6), SMC-SIGN can be obtained as follows:

$$u = -\frac{4m}{\mu_0 A N^2}\left\{[-\xi \mathrm{sgn}(s) - ks] - c[x_2(t) - x_{d_2}(t)] - \left(g + \frac{f_d}{m} - \dot{x}_{d_2}(t)\right)\right\} \tag{7}$$

$$\mathrm{sgn}(x) = \begin{cases} 1, x > 0 \\ 0, x = 0 \\ -1, x < 0 \end{cases}$$

The nominal levitation clearance and the expected velocity of the electromagnets can be expressed as follows:

$$\mathbf{X} = [\, x_{d_1} \quad x_{d_2} \,]^T = [\, 8mm \quad 0 \,]^T$$

3.2. Modified sliding mode controllers

Since the electromagnet system remains velocity when reaching the sliding surface, it will traverse the sliding surface because of inertia effect. The switching control term ξsgn(s) makes the proposed non-linear sliding mode controller (equation (7)) discontinuous. Under ideal conditions, in order to ensure that the sliding mode trajectory of the actual magnetic suspension system converges gradually to the sliding mode surface, the discontinuous control law requires the system to continuously cross the sliding mode surface at high frequency. Obviously, the output frequency of the choppers and other electronic components is not infinitely high because of the restriction of physical properties. In addition, the inductance of electromagnet and time delay in the controlling units also induce control lag. Therefore, the actual control current cannot accurately follow the desired high frequency under the individual and coupled effects of inertia and the limit of the physical properties. Thus, it is difficult to fundamentally solve the problem of the SMC while improving the suppression ability of chattering.

The electromagnetic levitation system is naturally non-linear, and sliding mode chattering may exacerbate non-linearity, making the problem more complicated. High-frequency chattering is likely to excite unmodeled modes of the maglev vehicle, and the procreant harmonic resonance may lead to unwanted effects on the track or vehicle components, thus threatening the levitation stability. Thus, chattering suppression is the premise and key problem of the engineering application technology of SMC.

The exponential reaching term in Equation (6) ensures that the sliding mode trajectory can rapidly decay in the exponential form and reach the sliding mode surface without an overshoot, and the coefficient k is used to control the sliding mode convergence rate. The switching control term ξsgn(s) in Equation (6) is responsible for regulating the electromagnet state near the sliding mode surface; a proper coefficient ξ guarantees that the electromagnets can reach the nominal air clearance in a limited time. However, an excessive coefficient ξ may exacerbate chattering. Consequently, it is worth conducting a parameter analysis on non-linear controllers so as to conclude a parameter correction approach. At the same time, the chattering suppression ability of the non-linear SMC needs to be further strengthened.

The modified sliding mode controllers in this paper enhance the chattering suppression ability by replacing the general discontinuous control law with the continuous control law within the boundary layer. However, outside of the boundary layer, the algorithm still employs an isokinetic convergence term to ensure that the sliding mode trajectory is exponentially attracted to the surface. Specifically, the saturation function sat(s, μ) and the hyperbolic tangent function tanh (s, μ) are chosen to develop modified sliding mode algorithms.

1. The modified sliding mode controller using saturation function and exponential reaching law (SMC-SAT) is derived as follows:

$$u = -\frac{4m}{\mu_0 A N^2}\left\{[-\xi \mathrm{sat}(s,\mu) - ks] - c[x_2(t) - x_{d_2}(t)] - \left(g + \frac{f_d}{m} - \dot{x}_{d_2}(t)\right)\right\} \tag{8}$$

$$\dot{s} = -\xi \cdot \mathrm{sat}(s,\mu) - k \cdot s,\ \xi > 0, k > 0, \mu > 0$$

$$\mathrm{sat}(x) = \begin{cases} 1, x > \mu \\ \frac{x}{\mu}, |x| \le \mu \\ -1, x < \mu \end{cases}$$

2. The modified sliding mode controller using hyperbolic tangent function and exponential reaching law (SMC-TANH) is derived as follows:

$$u = -\frac{4m}{\mu_0 A N^2}\left\{[-\xi \tanh(s,\mu) - ks] - c[x_2(t) - x_{d_2}(t)] - \left(g + \frac{f_d}{m} - \dot{x}_{d_2}(t)\right)\right\} \tag{9}$$

$$\dot{s} = -\xi \cdot \tanh(s,\mu) - k \cdot s,\ \xi > 0, k > 0, \mu > 0$$

$$\tanh(x) = \frac{e^{\frac{x}{\mu}} - e^{-\frac{x}{\mu}}}{e^{\frac{x}{\mu}} + e^{-\frac{x}{\mu}}}$$

3.3. Stability

The proposed SMC-SIGN controller (shown in equation (7)), SMC-SAT controller (shown in equation (8)) and SMC-TANH controller (shown in equation (9)) can guarantee asymptotical stability of the maglev system.

Proof 1. A Lyapunov function is chosen as

$$V(x) = \frac{1}{2}s^2 \ge 0 \tag{10}$$

Taking the time derivative of $V(x)$, we can obtain

$$\dot{V}(x) = s \cdot \dot{s} \tag{11}$$

Substituting the sliding mode surface (equation (5)) and control laws (Equations (6), (8), (9)) to Equation (11).

For SMC-SIGN:

$$\dot{V}(x) = -s(\xi \mathrm{sgn}(s) + ks) = -s\xi \mathrm{sgn}(s) - ks^2 = -\xi|s| - ks^2 \le 0, \xi > 0, k > 0 \tag{12}$$

For SMC-SAT:

$$\dot{V}(x) = -s\xi \mathrm{sat}(s,\mu) - ks^2 \tag{13}$$

$$\begin{cases} s \cdot \mathrm{sat}(s,\mu) = |s| \ge 0, |s| > \mu \\ s \cdot \mathrm{sat}(s,\mu) = \frac{s^2}{\mu} \ge 0, |s| < \mu \end{cases}$$

It can be obtained as follows:

$$\dot{V}(x) = -s\xi \mathrm{sat}(s,\mu) - ks^2 \le 0, \xi > 0, k > 0 \tag{14}$$

For SMC-TANH:

$$\begin{aligned} \dot{V}(x) &= -s\xi \tanh\left(\frac{s}{\mu}\right) - ks^2 \\ &= -s\xi\left(1 - \frac{2}{e^{\frac{2s}{\mu}} + 1}\right) - ks^2 \\ &= -\xi \frac{1}{e^{\frac{2s}{\mu}} + 1} s\left(e^{\frac{2s}{\mu}} - 1\right) - ks^2 \le 0 \end{aligned} \tag{15}$$

where

$$\xi > 0, k > 0, \mu > 0$$

$$\begin{cases} s \ge 0, e^{\frac{2s}{\mu}} \ge 1 \\ s < 0, e^{\frac{2s}{\mu}} < 1 \end{cases}$$

$$s\left(e^{\frac{2s}{\mu}} - 1\right) \ge 0$$

Overall, the boundedness and convergence are proved. And the maglev vehicle can reach and remain on the sliding surface under the control of the three controllers.

4. Experimental platform and co-simulation model

In this study, a single-point levitation experimental platform and the related co-simulation model were constructed to determine the effectiveness of the improved modified sliding mode controllers.

4.1. Single-point levitation experimental platform

The structure of the single-point levitation experimental platform is shown in Figure 2, it consists of an electromagnet, a guideway, a sensor, a chopper controller, a DSPACE real-time control hardware (MICROLABBOX) and an upper control computer.

The levitation control system was constructed by Rapid Control Prototyping (RCP) technology. As shown in Figure 3, the sensor monitors the levitation clearance and acceleration of the electromagnet in real time and

subsequently transmits the status data to the chopper controller and MICROLABBOX. After analog-to-digital (A/D) conversion and transmission, MICROLABBOX calculates the expected current based on the compiled control algorithm, and then retransmits the control signals to the chopper controller. Finally, the chopper actuates electromagnetic levitation by emitting current.

In order to realize the real-time control and data monitoring, the upper control computer shall initially run the pre-designed GUI control interface in DSPACE Control Desk at the start of the experiment. The control interface is customized in accordance with the control algorithm, which is shown in Figure 3. Using the DSPACE Control Desk GUI, the computer monitors and controls the algorithm which is running in the MICROLABBOX.

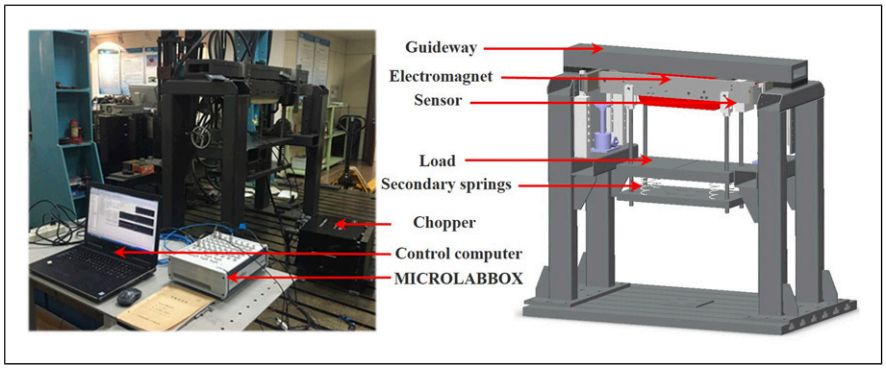

Figure 2. Experimental platform.

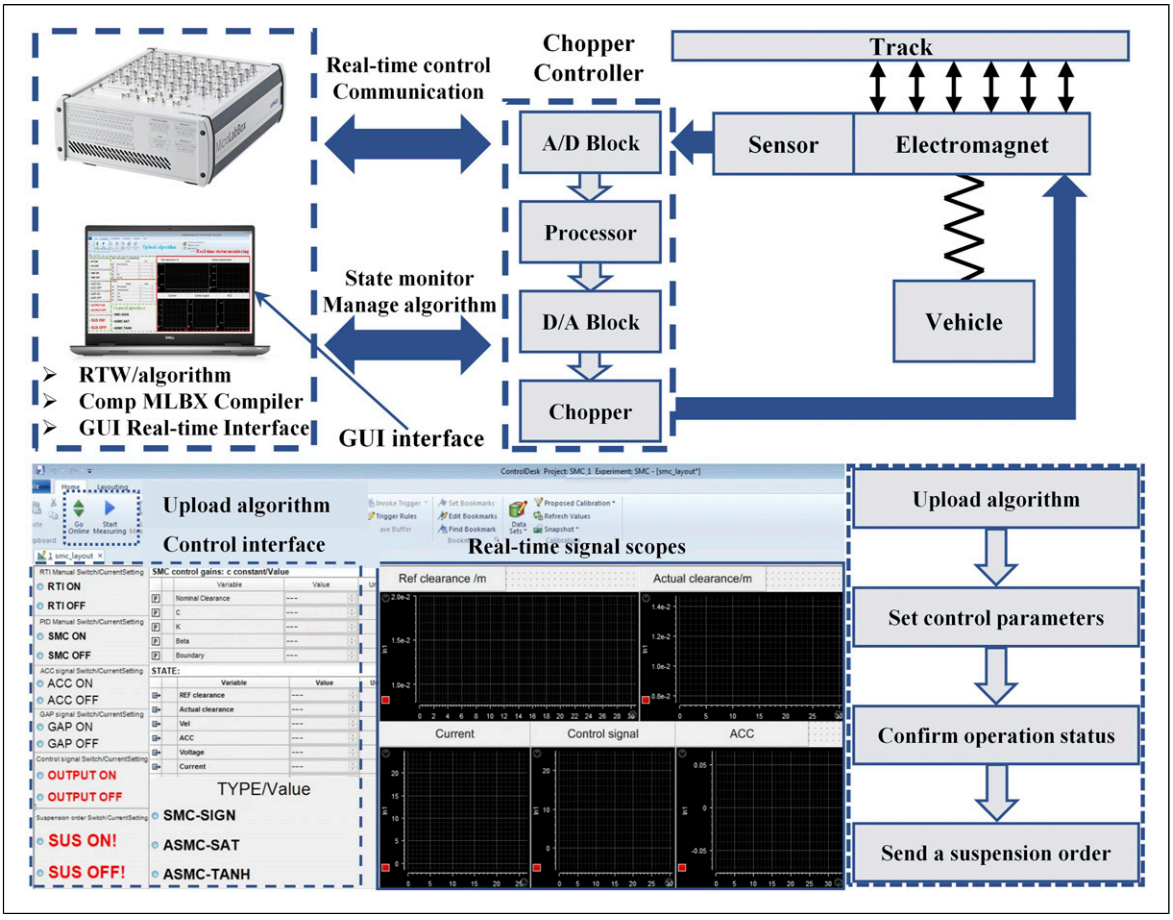

Figure 3. Schematic of the experimental platform control system.

4.2. The single-point levitation co-simulation model

Referring to the structures and control process of the single-point levitation experimental platform, a corresponding co-simulation model was established. As shown in Figure 4, the co-simulation model is divided into two modules, including the muti-body dynamics (MBD) module and the real-time control (RTC) module. At the beginning of each control loop, MBD module first collects clearance and acceleration of the magnet, and then transmits them to the RTC module. The RTC module will calculate the expected electromagnetic force according to the pre-defined algorithm. Afterwards, the RTC module outputs the solved electromagnetic force back to the MBD module. In accordance with this periodic process, the co-simulation model forms the feedback control of the single electromagnet dynamics model and actual embedded control algorithm.

The physical parameters which are consistent with the experimental platform are shown in Table 1.

In order to make the co-simulation model accurately simulate chattering phenomenon of maglev system under sliding mode control, we connected a low-pass filter in series at the output end of RTC module to simulate the comprehensive influence of the inductance, chopper performances. The time delay in the control loop is another major unavoidable factor that leads to chattering. Assuming that the effect of each time delay is reflected at the end, a zero-order holder is used to delay the output current.

In order to determine the cut-off frequency of the low-pass filter, the current of the electromagnet under PID control was recorded. Figure 5(a) showed the history of the actual current covering the whole process from transient state to steady state. Throughout the frequency analysis of the transient state (Part A and Part B) and steady state (Part C), as shown in Figure 5(b), the output current was dominated by low-frequency vibration in a unified way. This phenomenon proved that the hardware physical properties limited the output frequency. Following the analysis, the cut-off frequency of the low-pass filter was set as 100 Hz, which ensured that the dominant frequency is retained.

In the next section of parameter influence analysis, the influence of different degrees of the time delay were fully researched at first. Then, the time delay for the subsequent study was selected to be 3 ms, as it is common in maglev control systems and is big enough to induce chattering.

The effects of the low-pass filter and zero-order holder on chattering were simulated. As shown in Figure 6, there was no chattering in the absence of the low-pass filter and zero-order holder. However, when the low-pass filter or zero-order holder worked, chattering started to appear. It was concluded that the co-simulation model can effectively simulate actual chattering phenomenon resulting from inertia, time delay, inductance and restrictions of the hardware physical properties.

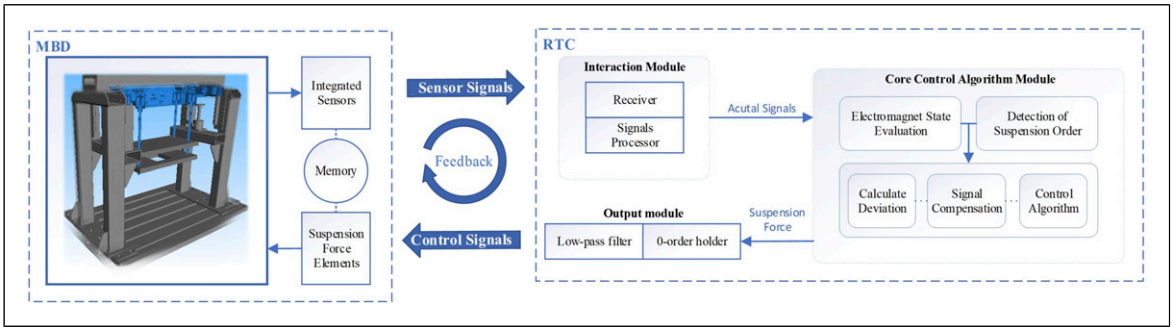

Figure 4. Schematic of the electromagnetic levitation co-simulation process.

Table 1. Physical parameters of the experimental platform and MBD model.

Parameter	Value	Units
Electromagnetic inductance	177.8	mH
Electromagnet mass with counterweight	178.3	kg
Nominal air clearance	8	mm
Electromagnetic impedance	0.420	Ω
Permeability in air	$4\pi \times 10^{-7}$	N/A^2
Effective electromagnet pole area	0.0163	m^2
Number of coil turns	360	

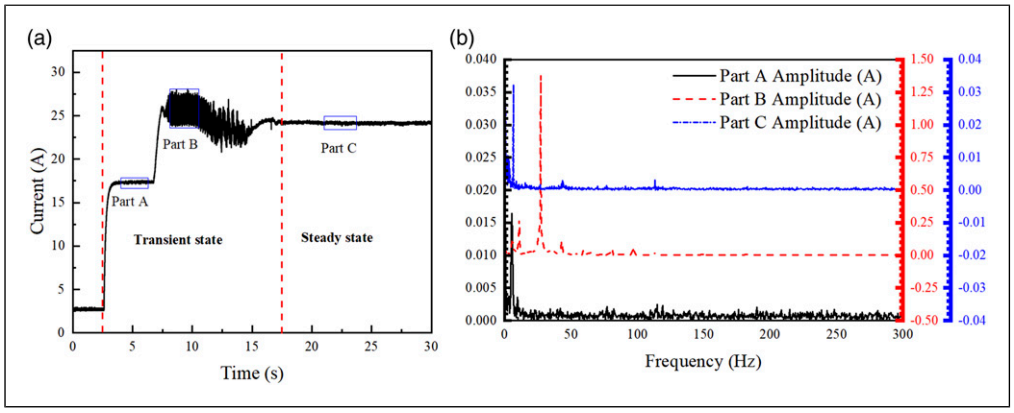

Figure 5. (a) Current in the whole process; (b) FFT results of all parts.

5. Parameter influence analysis

In this section, to study the relationship between the parameters c, k, ξ, μ and the performance of maglev system, parameter influence analysis of the above-mentioned three kinds of SMCs was performed using the co-simulation model.

5.1. Influence of time delay

Simulations were performed to study levitation stability with different levels of time delays. The involved controllers included SMC-SIGN, SMC-SAT and SMC-TANH, whose fixed control parameters were $c = 5$, $k = 10$ and $\xi = 1$.

Figure 7(a) depicts the fluctuations in the electromagnet chattering amplitude in the various controllers when the time delay was changed from 0 to 60 ms. It was evident that SMC-SIGN could not effectively suppress chattering because even a brief delay would produce chattering. Simultaneously, the amplitude increased fast with increasing time delay. However, SMC-SAT and SMC-TANH demonstrated superior control performance. Using the same control parameters as SMC-SIGN, SMC-SAT and SMC-TANH were able to suppress chattering induced by time delays ranging from 0 to 45 ms. In practical implementations, time delays originate from several modules of the maglev system, making it imprecise and unpredictable. Figure 7 demonstrates that SMC-SAT and SMC-TANH are more robust to application-related time delays than SMC-SIGN.

Since time delay has significant influence on system stability (including control), it is sometimes used to achieve a stable control deliberately. This section analyses the impact of time delay on the stability theoretically in order to guide the design of the sliding mode controller.

Let $z_\tau = z(t-\tau)$ and $z_\tau' = z'(t-\tau)$, they represent the clearance signal and velocity signal with time delay, τ respectively. By combining Equations (3) and (9), the single electromagnet suspension dynamic model under the control of SMC-TANH can be updated as follows:

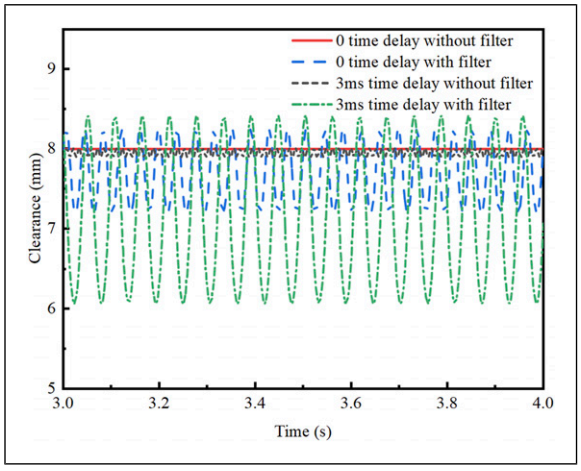

Figure 6. Effects of the low-pass filter and zero-order holder on chattering.

$$\ddot{z} = -\xi \tanh\left(\frac{s}{\mu}\right) - ks - c\left(\dot{z}_\tau - \dot{z}_{\tau d}\right) - \left(\frac{f_d}{m} - \ddot{z}_{\tau d}\right) \quad (16)$$

According to Equations (5) and (6), Equation (16) can be further simplified:

$$\begin{aligned} \ddot{z} &= -\xi \tanh\left(\frac{s}{\mu}\right) \\ &-k\left[c(z_\tau - z_{\tau d}) + \dot{z}_\tau - \dot{z}_{\tau d}\right] \\ &-c\left(\dot{z}_\tau - \dot{z}_{\tau d}\right) - \left(\frac{f_d}{m} - \ddot{z}_{\tau d}\right) \end{aligned} \quad (17)$$

where

$$\frac{s}{\mu} = \frac{c(z_\tau - z_{\tau d}) + \dot{z}_\tau - \dot{z}_{\tau d}}{\mu}$$

Considering the equilibrium position (z_d,0,0), Equation (17) can be converted to

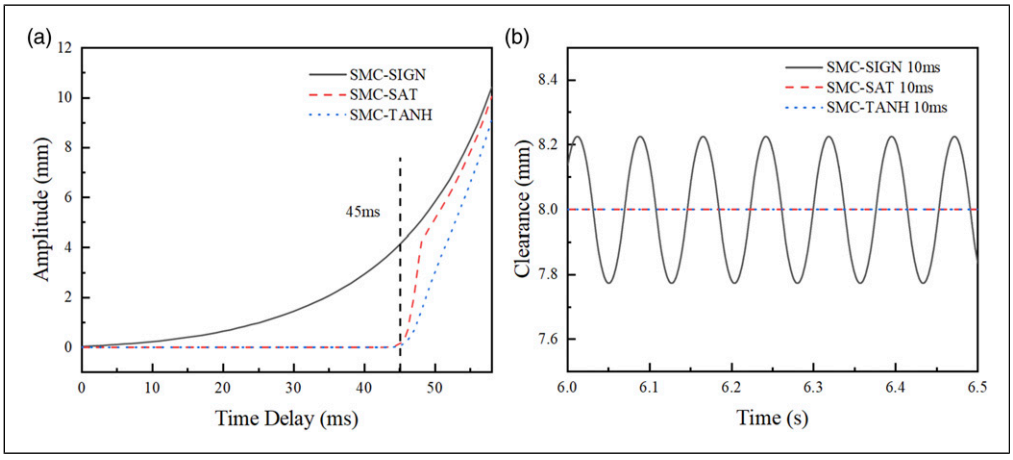

Figure 7. Comparison of SMC-SIGN, SMC-SAT and SMC-TANH in the case of different time delays: (a) Chattering amplitudes; (b) Time history of clearance when time delay is 10 ms.

$$\begin{aligned}\Delta\ddot{z} = &-\xi\tanh\left(\frac{c\Delta z_\tau + \Delta\dot{z}_\tau}{\mu}\right)\\ &-(k+c)\Delta\dot{z}_\tau - kc\Delta z_\tau - \frac{f_d}{m}\end{aligned} \tag{18}$$

In the formula above

$$\begin{cases}\Delta z = z - z_d\\ \Delta\dot{z} = \dot{z}\\ \Delta\ddot{z} = \ddot{z}\end{cases}$$

To study the stability of the maglev system near the nominal clearance, it is necessary to perform a linear expansion of Equation (18) near the equilibrium point to examine the stabilities of the tractable solutions.

$$\Delta\ddot{z} + \left(k + c + \frac{\xi}{\mu}\right)\Delta\dot{z}_\tau + \left(\frac{c\xi}{\mu} + kc\right)\Delta z_\tau + \frac{f_d}{m} = 0 \tag{19}$$

The corresponding characteristic equation of the linearized system can be obtained.

$$D(\lambda,\tau) = a_0\lambda^2 + b_0\lambda e^{-\lambda\tau} + c_0 e^{-\lambda\tau} + d_0 = 0,$$
$$(c>0, k>0, \xi>0, \mu>0)\begin{cases}a_0 = 1\\ b_0 = k + c + \dfrac{\xi}{\mu}\\ c_0 = \dfrac{c\xi}{\mu} + kc\\ d_0 = \dfrac{f_d}{m}\end{cases} \tag{20}$$

Let the complex number $\lambda = \alpha + i\,\beta$ ($\beta > 0$) be the root of Equation (20). After substituting the root into the characteristic equation with time delay, the real and imaginary parts can be extracted.

$$\begin{cases}a_0(\alpha^2 - \beta^2) + b_0 e^{-\alpha\tau}(\alpha\cos(\beta\tau) + \beta\sin(\beta\tau))\\ \quad + c_0 e^{-\alpha\tau}\cos(\beta\tau) + d_0 = 0\\ 2a_0\alpha\beta + b_0 e^{-\alpha\tau}(\beta\cos(\beta\tau)\\ \quad - \alpha\sin(\beta\tau)) - c_0 e^{-\alpha\tau}\sin(\beta\tau) = 0\end{cases} \tag{21}$$

When a pair of co-choked imaginary roots crossing the imaginary axis ($\lambda = \pm i\beta$), the stability of the system changes at the equilibrium point. And this is a sufficient condition for the appearance of the Hopf bifurcation. Let $\alpha = 0$, Equation (21) can be simplified as

$$\begin{cases}-a_0\beta^2 + b_0\beta\sin(\beta\tau) + c_0\cos(\beta\tau) + d_0 = 0\\ b_0\beta\cos(\beta\tau) - c_0\sin(\beta\tau) = 0\end{cases} \tag{22}$$

Equation (22) is the stable boundary of the system at the ordinary immobile point. By eliminating $\sin(\beta\tau)$ and $\cos(\beta\tau)$, the equation of β_0 can be solved.

$$\beta^4 - (2d_0 + b_0^2)\beta^2 + d_0^2 - c_0^2 = 0 \tag{23}$$

Assuming no disturbance in the system, $d^2 - c^2 < 0$ can be solved by combining Equation (20). Based on the relationship between roots and coefficients, there are always positive roots in Equation (23). And Equation (20) always has a pair of conjugate pure imaginary roots, the corresponding time delay is shown below.

$$\tau_j = \frac{1}{\beta_0}\arccos\left(\frac{a_0c_0\beta_0^2 - c_0d_0}{b_0^2\beta_0^2 + c_0^2} + 2jt\right), j = 0, 1, 2, \cdots \tag{24}$$

When the Hopf bifurcation occurs, the pair of conjugate pure imaginary eigenvalues cross the imaginary axis at a non-zero velocity. Therefore, the crossing condition of the eigenvalues are checked.

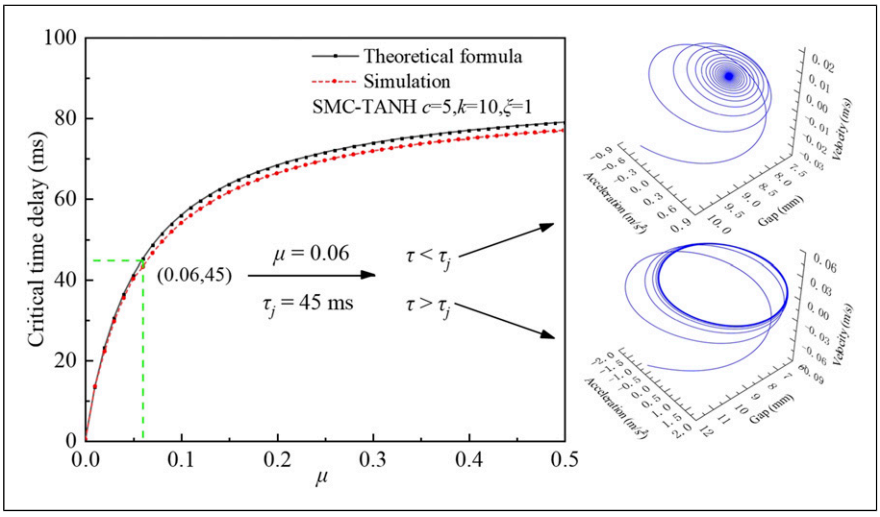

Figure 8. Relationship between critical time delay and boundary layers.

$$\mathrm{Re}\left(\frac{d\lambda}{d\tau}\right)_{\tau=\tau_0}^{\lambda=i\beta_0} = \frac{p\cdot pp + q\cdot qq}{pp^2 + qq^2} \neq 0$$

$$\begin{cases} p = \beta_0^2 b\cos\tau_j\beta_0 - \beta_0 c\sin\tau_j\beta_0 \\ q = \beta_0^2 b\sin\tau_j\beta_0 + \beta_0 c\cos\tau_j\beta_0 \\ pp = b\cos\tau_j\beta_0 - b\tau_j\beta_0\sin\tau_j\beta_0 - c\tau_j\cos\tau_j\beta_0 \\ qq = -b\sin\tau_j\beta_0 - b\tau_j\beta_0\cos\tau_j\beta_0 + c\tau_j\sin\tau_j\beta_0 + 2a\beta \end{cases} \tag{25}$$

Figure 8 compares the critical time delays of the co-simulation and theoretical models with various boundary layers using the same control parameters ($c = 5$, $k = 10$ and $\xi = 1$). The numerical and theoretical conclusions remain in good accord with the boundary layer's alterations. It states that the time delay boundary grows as the boundary layer thickness μ increases. When the parameter is below the curves, the normal solution is asymptotically stable. These curves also identify the locations where Hopf bifurcation and chattering occur. Particularly for the scenario depicted in Figure 7 ($\mu = 0.06$ $\tau_j = 45$ ms), the maglev system is stable prior to the critical time delay. Chattering appears after the critical time delay, as depicted in Figure 8.

5.2. Influence of the boundary layer μ

A proper boundary layer can balance the control accuracy and chattering suppression ability. The electromagnet responses (chattering amplitudes in the stable state) for different boundary layers were compared in Figure 9, and SMC-SAT and SMC-TANH shared the same fixed parameters ($c = 5$, $k = 10$, $\xi = 1$). It was evident that SMC-SAT and SMC-TANH shared an identical minimum boundary layer μ_0, where chattering could be completely suppressed.

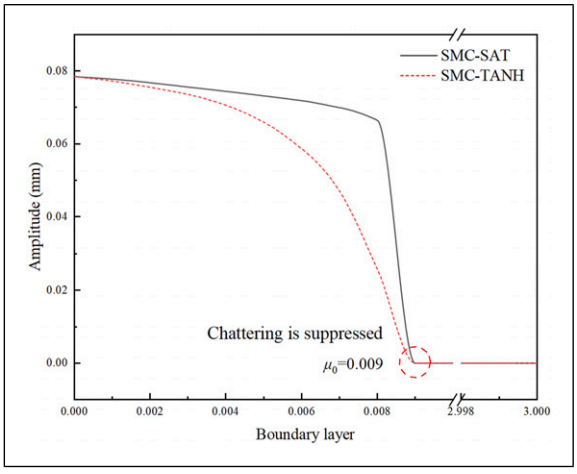

Figure 9. Comparison of SMC-SAT and SMC-TANH in the case of different boundary layers: Dependence of chattering amplitude on boundary layer.

Besides, SMC-TANH can suppress more chattering than SMC-SAT when $\mu < \mu_0$.

5.3. Influence of the control parameters

The influence of the sliding surface coefficient c, exponential reaching term coefficient k and switching control term coefficient ξ on chattering was studied. Firstly, Figure 10(a) presented the effect of the slide surface coefficient c and switching control term coefficient ξ on the chattering amplitude in SMC-SIGN, SMC-SAT and SMC-TANH separately. And Figure 10(b) highlighted the dependence of chattering amplitude on ξ by comparison. Figure 10 revealed that, at equilibrium, control parameters could greatly affect the performance of SMC-SIGN. Similarly, the increase in c, k and ξ might easily cause the maglev

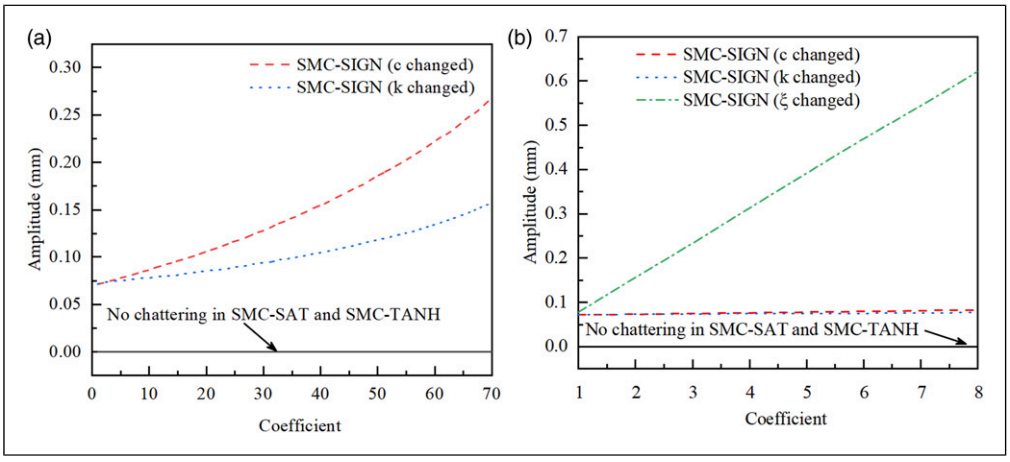

Figure 10. Comparison of SMC-SIGN, SMC-SAT and SMC-TANH in the case of different parameters: (a) Dependence of chattering amplitude on c and k; (b) Dependence of chattering amplitude on ξ.

system to descend into a more violent chattering. Moreover, the influence of ξ is significantly bigger than the effects of c and k. With a good boundary layer, SMC-SAT and SMC-TANH were able to suppress the chattering, and the controllers were robust to parameter change. Consequently, SMC-SAT and SMC-TANH are better suited for practical applications when accompanied by proper control parameters.

6. Adaptive correction method of SMC parameters

Numerical simulation above mentioned shows that the changes of the boundary layer μ and switching control term coefficient ξ can improve chattering suppression ability of SMC efficiently. An adaptive correction method of SMC parameters, which can find the proper control parameters online to trade-off the accuracy and robustness, is herein proposed to enhance the adaptability of modified sliding mode controllers in different environments. Specially, algorithm will find the minimum boundary layer on top of fully tunning the switching control term because the control accuracy decreases with increasing μ (Slotine and Li, 2006). The module is independently arranged at the output end, and the logic diagram is present in Figure 11. Within each control loop, the module is divided into a feedback block and a correction block. The feedback block continuously monitors the clearance and determines the existence of chattering. If chattering exists, the correction block will be activated to search the proper control parameters depending on the algorithm and the non-linear boundary.

To ensure the legality of parameters during real-time regulation, ξ should satisfy Equations (7), (8) and (9) with the fixed parameters c and k.

$$u(t) = -\frac{4m}{\mu_0 A N^2}\left\{[-\xi \mathrm{fun}(s,\mu) - ks] - c[x_2(t) - x_{d_2}(t)] - \left(g - \dot{x}_{d_2}(t)\right)\right\} \tag{26}$$

According to Equation (3),

$$u(t) = \frac{i(t)^2}{x_1(t)^2} \geq 0 \tag{27}$$

Since the sensors can measure the electromagnet real-time state, the non-linear relations between control parameters can be solved by combing Equation (26) and Equation (27).

$$\xi \cdot \mathrm{fun}(s,\mu) \geq -ks - cx_2 + cx_{d_2} - g + \dot{x}_{d_2}, \xi \geq 1, \mu > 0 \tag{28}$$

where fun(·) represents the SIGN, SAT or TANH. If ξ exceeds the non-linear boundary, the correction block autonomously changes the parameter to the boundary preventing danger.

The adaptive SMC-SAT (ASMC-SAT) and adaptive SMC-TANH (ASMC-TANH) were developed, and the effectiveness and superiority were proved by comparison with SMC-SIGN, SMC-SAT. Besides, the initial control parameters were improperly set in view of parameter mismatch. The temporal history of levitation clearance in SMC-SIGN, SMC-SAT and ASMC-SAT was displayed in Figure 12(a), and the real-time changes of μ and ξ were shown in Figure 12(b). It was evident form Figure 12(a) that only ASMC-SAT could solve the chattering issue flawlessly and ensure that the electromagnets levitated at the nominal clearance (8.0 mm). Specifically, the ASMC-SAT was comprised of four basic stages. In the first stage, as shown in Figure 12(b), ASMC-SAT rapidly adapted

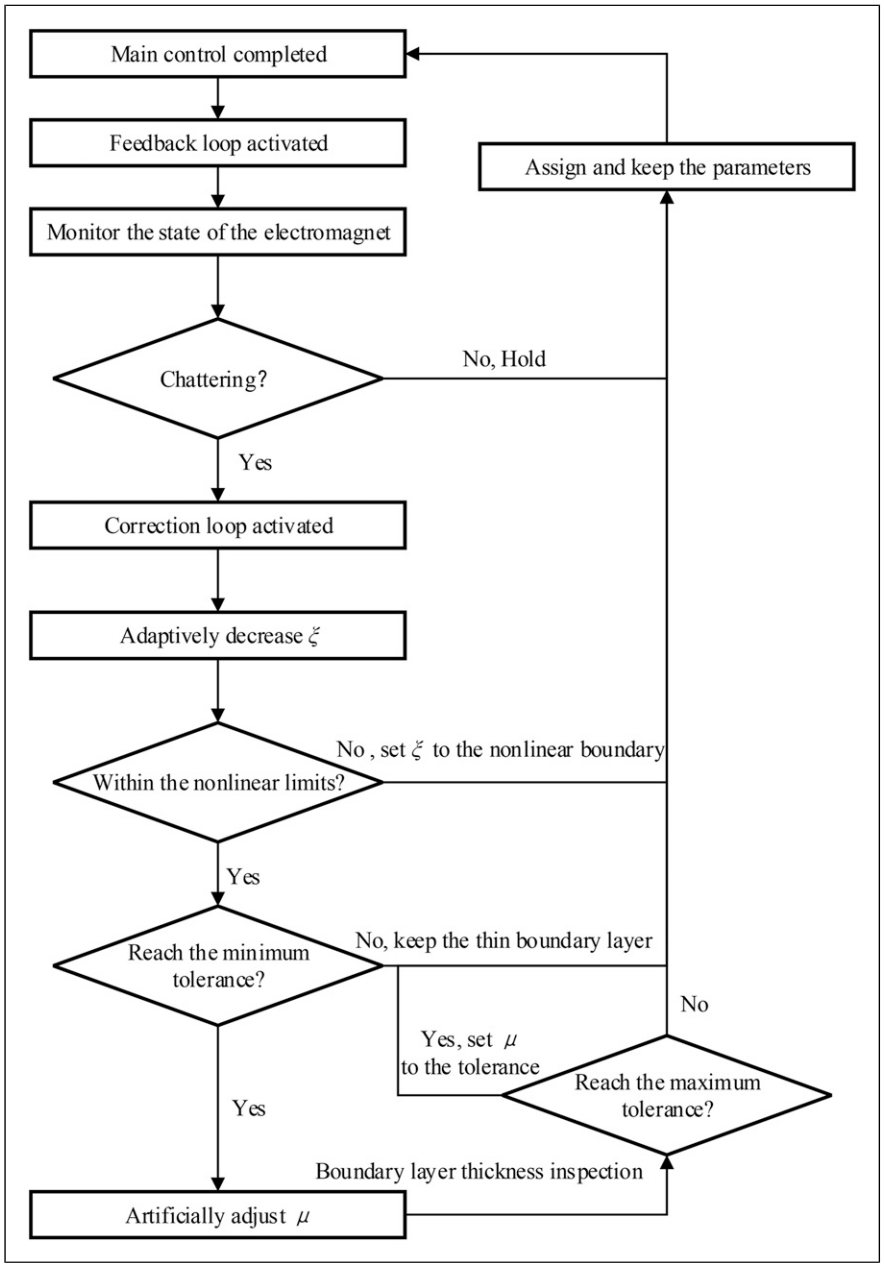

Figure 11. Logic diagram of the adaptive correction method for SMC parameters.

the large ξ from 10.0 to 4.4 in 0.045 s for the non-linear boundary Equation (28). When the maglev system entered the steady state for a while, ASMC-SAT adaptively adjusted ξ to the minimum tolerance (1.0) in the second stage. Figure 12(a) demonstrated that most of the chattering was suppressed here (0.4–0.1 mm). In the third stage, the remaining part was entirely filtered with the increase of μ. Eventually, in the fourth step, the electromagnet could levitate without chattering. Thus, ASMC-SAT had superior security and chattering suppression characteristics compared to SMC-SIGN and SMC-SAT.

7. Levitation experiments

The control performances of SMC-SIGN, ASMC-TANH and ASMC-SAT were experimentally compared based on the single-point levitation experimental platform.

Figure 13 showed the time history curves of the measured levitation clearance, corresponding current and acceleration in SMC-SIGN, ASMC-SAT and ASMC-TANH separately. At the beginning stage (0–5 s), as shown in Figure 13, the electromagnet under SMC-SIGN converged to the nominal clearance in chattering with a 29.5A high current overshot. While ASMC-SAT and

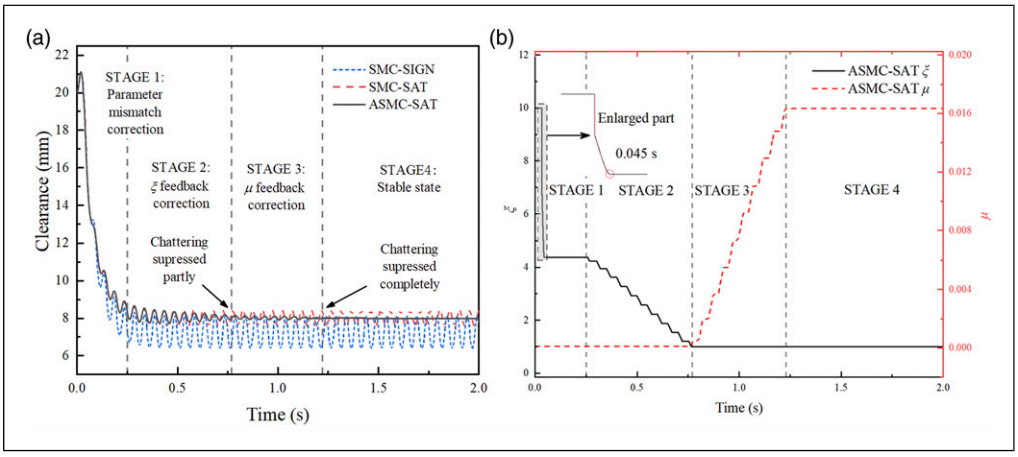

Figure 12. Effects of the adaptive correction method of SMC parameters: (a) levitation clearance in SMC-SIGN, SMC-SAT and ASMC-SAT; (b) real-time parameter ξ and μ changes in ASMC-SAT.

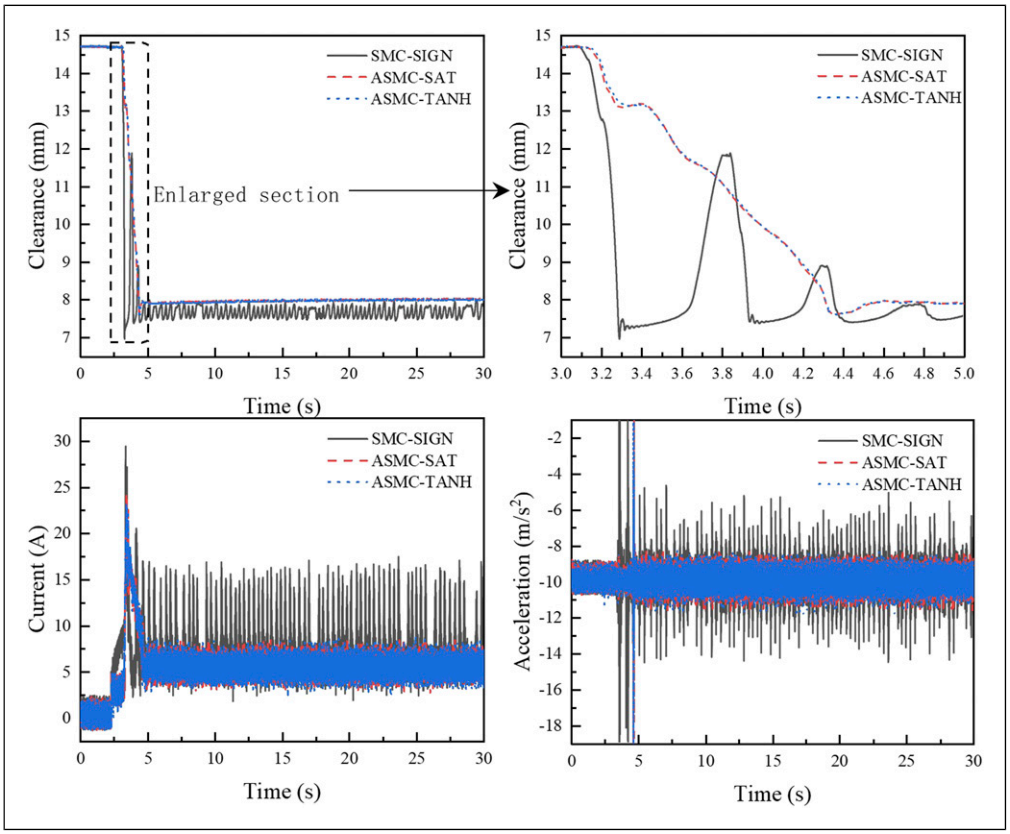

Figure 13. Time history curves of the levitation experiments.

ASMC-TANH suppressed chattering and levitated the electromagnet smoothly. Furthermore, there was chattering in the levitation system of SMC-SIGN near the nominal clearance: SMC-SIGN resulted in high-frequency chattering around 7.7 mm, with an amplitude of 0.24 mm. Nevertheless, ASMC-SAT and ASMC-TANH could effectively suppress chattering amplitudes to 0.011 mm and 0.009 mm, respectively. The current and acceleration variations of ASMC-TANH were fewer than those of ASMC-SAT and significantly lower than those of SMC-SIGN at equilibrium. In conclusion, ASMC-SAT and ASMC-TANH demonstrated superior control performance

compared to SMC-SIGN and were able to effectively suppress actual chattering.

8. Conclusion

This paper focused on the chattering problem of maglev vehicle sliding mode controllers. Firstly, the single-point dynamics model was established, and then the improved sliding mode controllers were designed based on the exponential reaching law and continuous switch item. Then, the experimental platform and corresponding co-simulation model were introduced. At the co-simulation model output, a low-pass filter and zero-order holder were connected in series in order to properly simulate the chattering in the practical maglev system under SMC. Using the co-simulation model, the influences of control parameters on chattering were analysed. On the basis of the analysis, an adaptive correction method of SMC parameters was proposed, and the adaptive SMC-SAT and SMC-TANH were obtained. In the end, the effectiveness of proposed ASMC-SAT and ASMC-TANH were verified on the experimental platform.

Overall, the modified ASMC-SAT and ASMC-TANH performed better than SMC-SIGN, and the performance of the former two was sufficient to cause electromagnets to levitate without actual chattering. This research can give a theoretical foundation and experimental data for the implementation of SMC in maglev system.

Declaration of Conflicting Interests

The author(s) declared no potential conflicts of interest with respect to the research, authorship and/or publication of this article.

Funding

The author(s) disclosed receipt of the following financial support for the research, authorship and/or publication of this article: The project was supported by the CAS Project for Young Scientists in Basic Research (Grant YSBR-045) and the National Natural Science Foundation of China (Grant 51805522).

ORCID iD

Han WU https://orcid.org/0000-0002-8450-0023

References

Bartolini G, Ferrara A and Usai E (1998) Chattering avoidance by second-order sliding mode control. *IEEE Transactions on Automatic Control* 43: 241–246.

De Boeij J, Steinbuch M and Gutierrez H (2006) Real-time control of the 3-DOF sled dynamics of a null-flux maglev system with a passive sled. *IEEE Transactions on Magnetics* 42: 1604–1610.

Eroglu Y and Ablay G (2016) Cascade sliding mode-based robust tracking control of a magnetic levitation system. *Proceedings of the Institution of Mechanical Engineers Part I-Journal of Systems and Control Engineering* 230: 851–860.

Ferrara A, Incremona GP and Sangiovanni B (2019) Tracking control via switched integral sliding mode with application to robot manipulators. *Control Engineering Practice* 90: 257–266.

Li M, Luo S, Ma W, et al. (2020) Experimental and numerical investigations of the dynamic responses of low and medium speed maglev train-track-bridge coupled system. *Vehicle System Dynamics* 60: 1555–1578.

Roy RG and Ghoshal D (2021) A novel adaptive second-order sliding mode controller for autonomous underwater vehicles. *Adaptive Behavior* 29: 39–54.

Slotine J and Li WP (2006) *Applied Nonlinear Control*. China Machine Press.

Slotine JJE (1984) Sliding controller-design for non-linear systems. *International Journal of Control* 40: 421–434.

Su YX, Zheng CH and Duan BY (2005) Automatic disturbances rejection controller for precise motion control of permanent-magnet synchronous motors. *Ieee Transactions on Industrial Electronics* 52: 814–823.

Sun YG, Xu JQ, Qiang HY, et al. (2019a) Adaptive sliding mode control of maglev system based on RBF neural network minimum parameter learning method. *Measurement* 141: 217–226.

Sun YG, Xu JQ, Qiang HY, et al. (2019b) Adaptive neural-fuzzy robust position control scheme for maglev train systems with experimental verification. *IEEE Transactions on Industrial Electronics* 66: 8589–8599.

Sun YG, Xu JQ, Wu H, et al. (2021) Deep learning based semi-supervised control for vertical security of maglev vehicle with guaranteed bounded airgap. *IEEE Transactions on Intelligent Transportation Systems* 22: 4431–4442.

Wang L, Deng Z, Wang H, et al. (2020a) Dynamic responses of HTS maglev system under track random irregularity. *IEEE Transactions on Applied Superconductivity* 30: 1–7.

Wang X, Zhang Y and Gao P (2020b) Design and analysis of second-order sliding mode controller for active magnetic bearing. *Energies* 13: 5965.

Wu H, Zeng XH and Gao DG (2020a) periodic response and stability of a maglev system with delayed feedback control under aerodynamic lift. *International Journal of Structural Stability and Dynamics* 21: 2150040.

Wu H, Zeng XH, Gao DG, et al. (2021) Dynamic stability of an electromagnetic suspension maglev vehicle under steady aerodynamic load. *Applied Mathematical Modelling* 97: 483–500.

Wu H, Zeng XH, Lai J, et al. (2020b) Nonlinear hunting stability of high-speed railway vehicle on a curved track under steady aerodynamic load. *Vehicle System Dynamics* 58: 175–197.

Xu J, Sun Y, Gao D, et al. (2018) Dynamic modeling and adaptive sliding mode control for a maglev train system based on a magnetic flux observer. *Ieee Access* 6: 31571–31579.

Zeng XH, Shi HM and Wu H (2021) Nonlinear dynamic responses of high-speed railway vehicles under combined self-excitation and forced excitation considering the influence of unsteady aerodynamic loads. *Nonlinear Dynamics* 105: 3025–3060.